J Electr Eng Technol.2018; 13(4): 1494-1503
http://doi.org/10.5370/JEET.2018.13.4.1494

ISSN(Print) 1975-0102
ISSN(Online) 2093-7423

Probabilistic Load Flow for Power Systems with Wind Power Considering the Multi-time Scale Dispatching Strategy

Chao Qin†, Yixin Yu* and Yuan Zeng*

Abstract – This paper proposes a novel probabilistic load flow model for power systems integrated with large-scale wind power, which considers the multi-time scale dispatching features. The ramp limitations of the units and the steady-state security constraints of the network have been comprehensively considered for the entire duration of the study period; thus, the coupling of the system operation states at different time sections has been taken into account. For each time section, the automatic generation control (AGC) strategy is considered, and all variations associated with the wind power and loads are compensated by all AGC units. Cumulants and the Gram–Charlier expansion are used to solve the proposed model. The effectiveness of the proposed method is validated using the modified IEEE RTS 24-bus system and the modified IEEE 118-bus system.

Keywords: Wind power, Probabilistic load flow, AGC, Multi-time, Cumulants, Gram-Charlier expansion.

1. Introduction

Wind power generation, as one of the most technology-mature renewable energy generations with great development potential, is being developed rapidly around the world. Compared to conventional power generations, the important features of wind power generation are its intermittency, variability, and uncertainty. At present, it is difficult to forecast the output of wind power generation, with high precision [1]. The large-scale integration of wind power brings more uncertainties to the power system, and complicates its operation. Deterministic analysis methods have been unable to meet the needs of security analysis for power systems with large-scale wind power integration, owing to their inability to consider the uncertainties in wind power and loads [2]. The probabilistic load flow (PLF), which is one of the core parts of the probabilistic security assessment, can provide probabilistic distributions of the operation states of power systems under a variety of uncertainty factors and plays highly significant roles in the operation and planning of power systems [3-6].

In 1974, Borkowsk first put forward the concept of PLF [7]. Thereafter, several scholars conducted extensive research on the modeling and solution of PLF. The existing methods can be roughly divided into three groups-Monte Carlo simulation (MCS) methods, approximate methods, and analytical methods. For MCS methods [8-9], the cumulative distribution functions (CDF) and the probability density functions (PDF) of the voltage magnitude, voltage phase angle, and branch power flow can be statistically obtained. MCS methods feature strong adaptability to a variety of complex probability distribution models. However, it is difficult to use MCS methods in actual power systems owing to their requirement of a large amount of calculations. Approximate methods such as the point-estimate method [10-12] and the first-order second-moment method [13], approximately describe the statistical characteristics of the system state variables by utilizing the digital features of the input random variables. Compared with the MCS methods, the approximate methods have a significant advantage of fast calculation speed. However, these methods also demonstrate some disadvantages, such as the calculation accuracy of the point-estimate method may be limited owing to its inability to obtain an accurate high-order moment when the PDFs are complex, and the first-order second-moment method is often unable to obtain the probability distributions of the state variables. In analytical methods, the state variables are expressed as linear combinations of the input random variables, with the help of certain simplified methods including the convolution method [14-15] and the cumulant-based method [16-18]. The advantages of analytical methods are quick computing speed and the ability to obtain the probability distributions of the state variables. However, owing to the linearization approach used in these methods, the calculation accuracy may be low when the ranges of the input random variables are wide.

With the fast development of wind power, PLF of the power systems integrated with wind power has received much focus [19-23]. However, in the previous studies on PLF, the implicit assumption was that all variations associated with wind power and loads were compensated by the slack bus alone, which is obviously not consistent with the actual operation of the power systems [24].

† Corresponding Author: Key Laboratory of Smart Grid of Ministry of Education, Tianjin University, China. (qinchao@tju.edu.cn)
* Key Laboratory of Smart Grid of Ministry of Education, Tianjin University, China.
Received: June 10, 2017; Accepted: April 3, 2018

Especially, with the large-scale integration of wind power, there will be great variations in power systems, which may cause large deviations in the results.

Furthermore, because of the intermittency, variability, and uncertainty of wind power, there is a higher requirement for the peak regulation and frequency modulation abilities of the system and the load tracking ability of units. Constrained by the ramp ability limits of conventional units, the operation states of power systems at different time sections couple closely with each other. In previous studies, the expectations, standard deviations, and probability distributions of the system state variables were generally calculated under the condition that the probability distributions of the wind power output and loads are given for a time section. Therefore, these methods did not take the coupling of the system operation states in different time sections into account.

To solve these issues, a novel probabilistic load flow model is proposed, which considers the multi-time scale dispatching features of power systems integrated with wind power. The main characteristics of the proposed method are: (1) For a given wind power output curve and load curve, the base active power output levels of all conventional units are determined in the generation scheduling settlement, which considers the ramp limitations of units and the network steady-state security constraints; thus, the coupling of different time sections is taken into account in the PLF; (2) For each time section, the features of the automatic generation control (AGC) strategy are considered; therefore, the variations caused by the wind power and loads are reasonably assigned to the AGC units, which helps to overcome the defect that, in PLF calculation, all variations are compensated by the slack bus alone; (3) As the bus power injections are not independent, the relationships between the forecast errors of wind power and loads and the variations of operation variables is built up, based on which, cumulants and the Gram-Charlier expansion are used to solve the proposed PLF model.

The remainder of this paper is organized as follows: Section 2 describes the theoretical background of the PLF method based on cumulants and the Gram-Charlier expansion. The proposed PLF method is introduced in detail in Section 3. The numerical simulation results and explanations are presented in Section 4. Section 5 concludes the paper.

2. Basic Theories for PLF

2.1 Moments and cumulants

Moments and cumulants are two important digital characteristics of random variables. Assuming the PDF of a continuous random variable x to be $f(x)$, the kth-order moment α_k can be calculated using Eq. (1)

$$\alpha_k = \int_{-\infty}^{+\infty} x^k f(x)dx \tag{1}$$

The first-order moment of x is the expectation, namely, m. With the help of the expectation of the random variable, its kth-order central moment can be calculated using Eq. (2).

$$\beta_k = \int_{-\infty}^{+\infty} (x-m)^k f(x)dx \tag{2}$$

The cumulants of the random variables can be obtained with the help of the moments whose orders are not larger than that of the corresponding cumulants. The calculation is shown in Eq. (3). Where, γ_1, γ_{k+1} and γ_{k-j+1} are the cumulants of the random variable while the subscripts, i.e. 1, k+1 and k-j+1, are the cumulants' order; α_1, α_j and α_{k+1} are the moments of the random variable while the subscripts, i.e. 1, k+1 and j, are the moments' order.

$$\begin{cases} \gamma_1 = \alpha_1 \\ \gamma_{k+1} = \alpha_{k+1} - \sum_{j=1}^{k} C_k^j \alpha_j \gamma_{k-j+1}, k \geq 1 \end{cases} \tag{3}$$

The cumulants of independent random variables have the following important properties:

(1) Additivity: The all-order cumulants of the summation of the independent random variables are equal to the summation of the all-order cumulants of the random variables.

(2) Homogeneity: The kth-order cumulants of the random variable multiplied by a is equal to the kth-order cumulants of the variable, multiplied by a.

2.2 PLF based on cumulants and gram-charlier expansion

The power flow function can be expressed as in Eq. (4). In PLF calculation, the injection power $\boldsymbol{S}$ is generally regarded as a random variable. Once its probability distribution and the system topology are obtained, the expectation, variance, and probability distribution of the state variables ($\boldsymbol{X}$ and $\boldsymbol{Z}$) can be calculated.

$$\begin{aligned} \boldsymbol{S} &= \boldsymbol{f}(\boldsymbol{X}) \\ \boldsymbol{Z} &= \boldsymbol{g}(\boldsymbol{X}) \end{aligned} \tag{4}$$

According to the theory of Taylor Series, Eq. (4) can be linearized around the operating point ($\boldsymbol{S}_0$, $\boldsymbol{X}_0$), as shown in (5). $o_f(\Delta \boldsymbol{X})$ and $o_g(\Delta \boldsymbol{X})$ are high order infinitesimal of $\Delta \boldsymbol{X}$, which can be ignored when $\Delta \boldsymbol{X}$ is very small. $\frac{\partial \boldsymbol{f}}{\partial \boldsymbol{X}}$

and $\frac{\partial \boldsymbol{g}}{\partial \boldsymbol{X}}$ are the derivatives of $\boldsymbol{f}$ and $\boldsymbol{g}$ to $\boldsymbol{X}$. Since $\boldsymbol{S}_0 = \boldsymbol{f}(\boldsymbol{X}_0)$ and $\boldsymbol{Z}_0 = \boldsymbol{g}(\boldsymbol{X}_0)$, Eq. (5) can be reformed as (6). Further, $\Delta\boldsymbol{X}$ and $\Delta\boldsymbol{Z}$ can be expressed as a linear description of $\Delta\boldsymbol{S}$ through the transformation of (6), as shown in Eq. (7), where $\boldsymbol{J}_0 = \frac{\partial \boldsymbol{f}}{\partial \boldsymbol{X}}$ and $\boldsymbol{T}_0 = \frac{\partial \boldsymbol{g}}{\partial \boldsymbol{X}}\left(\frac{\partial \boldsymbol{f}}{\partial \boldsymbol{X}}\right)^{-1}$.

$$\begin{aligned} \boldsymbol{S}=\boldsymbol{S}_0+\Delta\boldsymbol{S}=\boldsymbol{f}(\boldsymbol{X}_0+\Delta\boldsymbol{X})=\boldsymbol{f}(\boldsymbol{X}_0)+\frac{\partial \boldsymbol{f}}{\partial \boldsymbol{X}}\Delta\boldsymbol{X}+o_f(\Delta\boldsymbol{X}) \\ \boldsymbol{Z}=\boldsymbol{Z}_0+\Delta\boldsymbol{Z}=\boldsymbol{g}(\boldsymbol{X}_0+\Delta\boldsymbol{X})=\boldsymbol{g}(\boldsymbol{X}_0)+\frac{\partial \boldsymbol{g}}{\partial \boldsymbol{X}}\Delta\boldsymbol{X}+o_g(\Delta\boldsymbol{X}) \end{aligned} \tag{5}$$

$$\begin{aligned} \Delta\boldsymbol{S}&=\frac{\partial \boldsymbol{f}}{\partial \boldsymbol{X}}\Delta\boldsymbol{X} \\ \Delta\boldsymbol{Z}&=\frac{\partial \boldsymbol{g}}{\partial \boldsymbol{X}}\Delta\boldsymbol{X} \end{aligned} \tag{6}$$

$$\begin{aligned} \Delta\boldsymbol{X}&=\boldsymbol{J}_0^{-1}\Delta\boldsymbol{S} \\ \Delta\boldsymbol{Z}&=\boldsymbol{T}_0\Delta\boldsymbol{S} \end{aligned} \tag{7}$$

Under the assumption that the elements of $\Delta\boldsymbol{S}$ are independent, according to the two properties of the cumulants of independent random variables, the all-order cumulants of $\Delta\boldsymbol{X}$ and $\Delta\boldsymbol{Z}$ can be obtained by the calculation of the all-order cumulants of $\Delta\boldsymbol{S}$, which is shown in Eq. (8).

$$\begin{aligned} \gamma_{\Delta\boldsymbol{X}}^k&=(\boldsymbol{J}_0^{-1})^k\gamma_{\Delta\boldsymbol{S}}^k \\ \gamma_{\Delta\boldsymbol{Z}}^k&=(\boldsymbol{T}_0)^k\gamma_{\Delta\boldsymbol{S}}^k \end{aligned} \tag{8}$$

Furthermore, through the relationship between the moments and cumulants of the random variables, the all-order moments of $\Delta\boldsymbol{X}$ and $\Delta\boldsymbol{Z}$ can be obtained.

The random variable ζ, with an expectation of μ and a standard deviation of σ, can be normalized as $\tau = (\zeta-\mu)/\sigma$. The distribution function of τ can be expressed as a Gram-Charlier expansion, as shown in Eq. (9). $\varphi(\tau)$ and $\Phi(\tau)$ are the PDF and the CDF, respectively, of the Gaussian distribution; $\varphi^i(\tau)$ and $\Phi^i(\tau)$ are the ith order derivatives of the corresponding functions. g_i is the coefficient of the ith order Gram–Charlier expansion and can be calculated using the all-order moments of the random variables. Related methods for calculating the Gram–Charlier expansions can be found in [16], and will not be explained here because of the paper length constraints.

$$\begin{aligned} f(\tau)&=\varphi(\tau)+\sum_{i=1}^{+\infty}g_i\varphi^i(\tau) \\ F(\tau)&=\Phi(\tau)+\sum_{i=1}^{+\infty}g_i\Phi^i(\tau) \end{aligned} \tag{9}$$

3. PLF Considering the Multi-time Dispatching Strategy for Wind Power

Generally, the forecast error of wind power will gradually increase with the prediction time. In practice, however, the integration and consumption of wind power are ensured by the dispatching strategy, which is coordinated in multi-time scales.

3.1 Uncertainty modeling of wind power and loads

As modern wind power generators are controlled using the maximum power point tracking strategy, the active power outputs of the wind farms are mainly determined by the wind speed. To characterize the uncertainty of wind power, an appropriate model is selected according to the study period or the temporal scale that is concerned.

The Weibull distribution can be fitted well to the medium and long-term features of wind speed; therefore, it is generally used for wind speed simulation in power system planning. The output power of the wind turbine can be obtained through the relationship between wind speed and the wind turbine output curve. In the study of the short-term uncertainty of wind power, the actual active power output of wind farms is generally expressed as the sum of the forecast value and the forecast error. The forecast error usually follows a Gaussian distribution with an average value of 0, as shown in Eq. (10).

$$P_i^{wr}(t)=P_i^{wf}(t)+\Delta e_i^w(t) \tag{10}$$

The actual loads are generally described as the sum of the load forecast values and the corresponding forecast errors, with the forecast errors following a Gaussian distribution, as shown in Eq. (11).

$$P_i^{dr}(t)=P_i^{df}(t)+\Delta e_i^d(t) \tag{11}$$

Although the forecast errors of wind farms and loads are modeled with Gaussian distribution in this paper, the proposed method can also apply for other distributions, such as beta distribution.

3.2 Dynamic economic dispatch for power systems with wind power

Once the forecast curves for wind power and loads in the future dispatching period are given, the total cost for power generation in the system can be minimized, by reasonably setting the active power outputs of conventional units. The specific model is shown as follows. Eq. (12) presents the objective function; Eq. (13) is the constraint equation for power balance in the system; Eq. (14) is the equation of the buses' active injection power; Eqs. (15) and (16) are the power flow equations; Eq. (17) is the constraint equation for the branch power flow; and Eq. (18) is the constraint equation for the units' ramping limitations.

$$\min \sum_{t=1}^{T}\left(\sum_{i\in\Omega_G}\left(a_i\left(P_i^G(t)\right)^2+b_iP_i^G(t)+c_i\right)\right) \tag{12}$$

$$\sum_{i\in\Omega_G} P_i^G(t) + \sum_{i\in\Omega_W} P_i^{wf}(t) = \sum_{i\in\Omega_D} P_i^{df}(t) \tag{13}$$

$$P_i = \sum_{j\in i} P_j^G(t) + \sum_{j\in i} P_j^{wf}(t) - \sum_{j\in i} P_i^{df}(t) \tag{14}$$

$$P_i - V_i \sum_{j\in i} V_j (G_{ij}\cos\theta_{ij} + B_{ij}\sin\theta_{ij}) = 0 \tag{15}$$

$$Q_i - V_i \sum_{j\in i} V_j (G_{ij}\sin\theta_{ij} - B_{ij}\cos\theta_{ij}) = 0 \tag{16}$$

$$\left|P_i^L(t)\right| \le P_i^{Lmax} \tag{17}$$

$$-\Delta r_i^{\max} \le P_i^G(t) - P_i^G(t-1) \le \Delta r_i^{\max} \tag{18}$$

3.3 AGC Regulation Model

During actual operation, the operation mode of the system will deviate from the scheduled operation mode because of the forecast errors of the wind power and loads. The imbalance power caused by wind power and load is shown in Eq. (19). Because the forecast errors of wind power and loads can be regarded as random variables, $\Delta P^s(t)$ is also a random variable.

$$\Delta P^s(t) = \sum_{i\in\Omega_W} \Delta e_i^w(t) - \sum_{i\in\Omega_D} \Delta e_i^d(t) \tag{19}$$

To maintain the power balance in the grid, the imbalanced power of the system is assigned to all units involved in the AGC regulation, as shown in Eq. (20).

$$\Delta P^s(t) + \sum_{i\in\Omega_{AG}} \Delta P_i^{AG}(t) = 0 \tag{20}$$

The AGC units share the imbalanced power according to their participation factors. Thus, the regulating power assigned to each AGC unit can be derived, as shown in Eq. (21).

$$\Delta P_i^{AG}(t) = -\alpha_i^{AG}\left(\sum_{i\in\Omega_W} \Delta e_i^w(t) - \sum_{i\in\Omega_D} \Delta e_i^d(t)\right) \tag{21}$$

Expressing Eq. (21) in a matrix form:

$$\Delta \boldsymbol{P}^{AG} = -\boldsymbol{\alpha}_{W2G}\Delta \boldsymbol{e}^W + \boldsymbol{\alpha}_{D2G}\Delta \boldsymbol{e}^d \tag{22}$$

$\Delta \boldsymbol{P}$, considering the AGC strategy can be calculated using Eq. (23).

$$\begin{aligned}\Delta \boldsymbol{P} &= \boldsymbol{M}_{G2B}\Delta \boldsymbol{P}^{AG} + \boldsymbol{M}_{W2B}\Delta \boldsymbol{e}^W - \boldsymbol{M}_{D2B}\Delta \boldsymbol{e}^d \\ &= \left[\boldsymbol{M}_{W2B} - \boldsymbol{M}_{G2B}\boldsymbol{\alpha}_{W2G} \quad \boldsymbol{M}_{G2B}\boldsymbol{\alpha}_{D2G} - \boldsymbol{M}_{D2B}\right]\begin{bmatrix}\Delta \boldsymbol{e}^W \\ \Delta \boldsymbol{e}^d\end{bmatrix}\end{aligned} \tag{23}$$

The premise for the PLF method based on cumulants and the Gram-Charlier expansion is the independence of the input random variables. Because the imbalanced power of the system is assigned to all AGC units, the active power outputs of the conventional units depend on the variations in the wind power and loads. Thus, the bus active power injections are not independent variables; rather, they are functions of the variations of wind power and loads. Therefore, the calculation method for PLF based on cumulants and the Gram-Charlier series cannot be applied directly.

By combining Eqs. (7) and (23), the variations of $\boldsymbol{X}$, i.e., the bus voltage magnitude and phase angle, and $\boldsymbol{Z}$, i.e., the branch power flow, can be expressed as functions of the forecast errors of wind power and loads, as shown in Eqs. (24) and (25).

$$\Delta \boldsymbol{X} = \boldsymbol{J}_0^{-1}\Delta \boldsymbol{P} = \boldsymbol{O}\begin{bmatrix}\Delta \boldsymbol{e}^W \\ \Delta \boldsymbol{e}^d\end{bmatrix} \tag{24}$$

$$\Delta \boldsymbol{Z} = \boldsymbol{T}_0\Delta \boldsymbol{P} = \boldsymbol{H}\begin{bmatrix}\Delta \boldsymbol{e}^W \\ \Delta \boldsymbol{e}^d\end{bmatrix} \tag{25}$$

$\boldsymbol{O}$ is the relation matrix describing the relationship between the forecast errors of wind power and loads and the bus voltage magnitude and phase angle, as shown in Eq. (26).

$\boldsymbol{H}$ is the relation matrix describing the relationship between the forecast errors of wind power and loads and the branch power flow, as shown in Eq. (27).

$$\boldsymbol{O} = \boldsymbol{J}_0^{-1}\left[\boldsymbol{M}_{W2B} - \boldsymbol{M}_{G2B}\boldsymbol{\alpha}_{W2G} \quad \boldsymbol{M}_{G2B}\boldsymbol{\alpha}_{D2G} - \boldsymbol{M}_{D2B}\right] \tag{26}$$

$$\boldsymbol{H} = \boldsymbol{T}_0\left[\boldsymbol{M}_{W2B} - \boldsymbol{M}_{G2B}\boldsymbol{\alpha}_{W2G} \quad \boldsymbol{M}_{G2B}\boldsymbol{\alpha}_{D2G} - \boldsymbol{M}_{D2B}\right] \tag{27}$$

As the forecast errors of wind power and loads are independent random variables, the cumulants of $\triangle\boldsymbol{X}$ and $\triangle\boldsymbol{Z}$ can be calculated using Eqs. (24) and (25).

From the above derivation, it can be inferred that the participation factor of each AGC unit represents the extent to which it is involved in the second frequency regulation, which will have an effect on the final power flow distribution of the system. The base outputs of the AGC units are determined by the short-term forecast of wind power and loads during the dispatch-making process. The base point and participation factor of each unit are the results of the optimized distribution of the planned total output, with a rolling optimization for every 15 min, and the values remain constant in each period. In practice, two setting modes are usually adopted. One is based on the regulating performance of each AGC unit, as shown in Eq. (28). The other is based on the available regulating capacity of each AGC unit, as shown in Eq. (29).

$$\alpha_i^{AG} = \frac{\Delta r_i^{max}}{\sum_{k\in\Omega_{AG}} \Delta r_k^{max}} \tag{28}$$

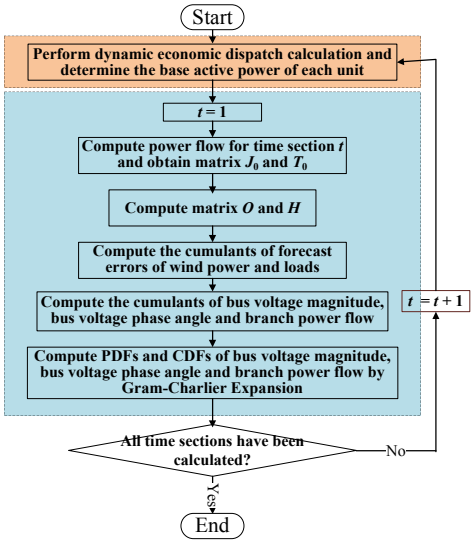

Fig. 1. Flowchart of the proposed method

$$\alpha_i^{AG} = \frac{P_i^{Gmax} - P_i^G}{\sum_{k \in \Omega_{AG}} (P_k^{Gmax} - P_k^G)} \tag{29}$$

3.4 Solution method

The proposed PLF method can be decoupled into two subproblems: one is a dynamic economic dispatch problem to determine the base active power of each unit, which is a nonlinear optimization problem solved by the Optimization Toolbox provided by MATLAB; the other is the expectation, variance, and probability distribution calculation of the system variables with consideration of the AGC strategy for a certain time section. The flow chart is shown in Fig. 1.

4. Case Study

4.1 The modified IEEE RTS 24-bus system

The IEEE RTS 24-bus system is used to verify the validity of the proposed method. Its diagram is shown in Fig. 2. Based on an original system, a wind farm with a capacity of 200 MW is integrated to bus 17, and its forecast output curve is extracted online form http://motor.ece.iit.edu/data/, which is shown in Fig. 3. Details of related parameters of the lines, loads, and generators can be found in [25], and details of the ramp rate limitations of the units can be found in [26]. Besides, the data of the system can be extracted online from https://www2.ee.washington.edu/research/pstca/. The standard deviation of the wind power forecast error is 10%, and that of the load forecast error is 3%. The units connected with bus 1, bus 2, bus 15, bus 16 and bus 22 are equipped with AGC regulation. Bus 13 is the slack bus.

In order to facilitate result comparison and analysis, and to validate the superiority of the proposed method, the

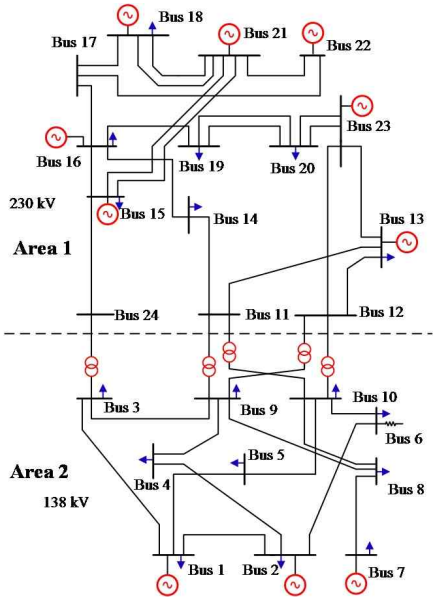

Fig. 2. The diagram of IEEE RTS 24-bus system

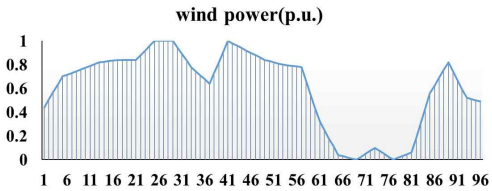

Fig. 3. The output curve of the wind farm

following four scenarios are considered.

Scenario A: Uses the method proposed in this paper and considers both AGC and the coupling of system states between different time sections;

Scenario B: Uses the conventional MCS method and considers both AGC and the coupling of system states between different time sections;

Scenario C: Uses the method proposed in this paper without considering the coupling of system states between different time sections;

Scenario D: Uses the method proposed in this paper without considering AGC.

The calculation efficiency and accuracy of the proposed method can be validated by the comparisons between **Scenario A** and **Scenario B**. The influence of the coupling of system states between different time sections can be analyzed by the comparisons between **Scenario A** and **Scenario C**. The influence of the AGC control strategy can be analyzed by the comparisons between **Scenario A** and **Scenario D.**

4.1.1 Results of comparison of scenario a and scenario B

Taking the results of MCS (Scenario B) as the base, the absolute error η_{ae} and the relative error η_{re} of the results obtained in Scenario A and Scenario B can be calculated. The calculation equation for η_{ae} is shown in (30) and the

calculation equation for η_{re} is shown in (31). ξ is a certain statistical characteristic of a random variable obtained through the proposed method; for example, the expectation of the bus voltage magnitude. ξ_{MC} is the corresponding statistical characteristic of the random variable obtained through the MCS method.

$$\eta_{ae} = \left|\xi - \xi_{MC}\right| \tag{30}$$

$$\eta_{re} = \left|\frac{\xi - \xi_{MC}}{\xi_{MC}}\right| \tag{31}$$

The sample size N in Scenario B is set to 5000. The calculation errors of the proposed method are shown in Table 1. It can be observed from Table 1 that the results of the proposed method demonstrate high calculation accuracy.

Both Scenario A and Scenario B are simulated using MATLAB and computed on a PC with a CPU frequency of 3.6 GHz and a memory of 8 GB. Under the same computing conditions, the computing time of the proposed method is 169.5s, while that of the MCS method is 6930.8s. Therefore, the computing time of the proposed method is only 2.45% of that of MCS. The main reason is that, for a certain time section, the AC power flow is calculated only once in the proposed method (to construct the matrixes $\boldsymbol{O}$ and $\boldsymbol{H}$). However, the AC power flow will be calculated N times in the MCS method (generally, to ensure the accuracy of the calculation results, the number N will be very large). Therefore, the proposed method has a significant advantage of computing speed over the MCS method.

Table 1. Calculation errors of the proposed method for IEEE RTS 24-bus system

	State variables	Characteristic variables	Average value	Maximum value
Absolute error	bus voltage magnitude (p.u.)	expectation	0.00000846	0.0000723
		standard deviation	0.00000284	0.0000275
	bus voltage phase angle (°)	expectation	0.0034	0.0288
		standard deviation	0.0021	0.0166
	branch active power (MW)	expectation	0.0409	0.4789
		standard deviation	0.0275	0.1976
	branch reactive power (MVar)	expectation	0.0824	0.9213
		standard deviation	0.0529	0.5537
Relative error	bus voltage magnitude (%)	expectation	0.000846	0.0074
		standard deviation	0.4225	2.903
	bus voltage phase angle (%)	expectation	0.0409	2.257
		standard deviation	0.77	3.302
	branch active power (%)	expectation	0.088	4.44
		standard deviation	0.8071	3.57
	branch reactive power (%)	expectation	0.127	3.61
		standard deviation	0.1943	3.02

4.1.2 Influence of the coupling of system states at different time sections

The system net load, i.e., the load-wind power output is shown in Fig. 4(a). The bus active power injection differences of Scenario A and Scenario C during the whole period are shown in Fig. 4(b). The horizontal axis of this figure is a timeline. The vertical axis of Fig. 4(b) is $P_i^A(t)$ - $P_i^C(t)$. Where $P_i^A(t)$ is the scheduled active power output of the ith generator bus in Scenario A, while $P_i^C(t)$ is the scheduled active power output of the ith generator bus in Scenario C. The figure shows that, when there is an obvious climbing process in the system net load curve (such as t=31, 65 and 67), there will be significant differences between the dispatching strategies of Scenario A and Scenario C. This is because the adjacent time sections are coupled with each other by the constraint of

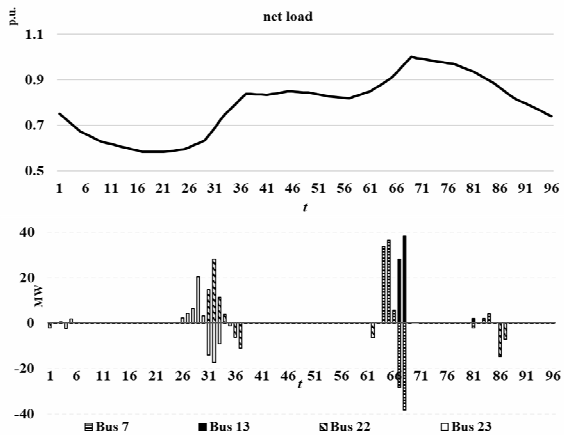

Fig. 4. Differences of the scheduled active power outputs of generation buses between scenario A and scenario C

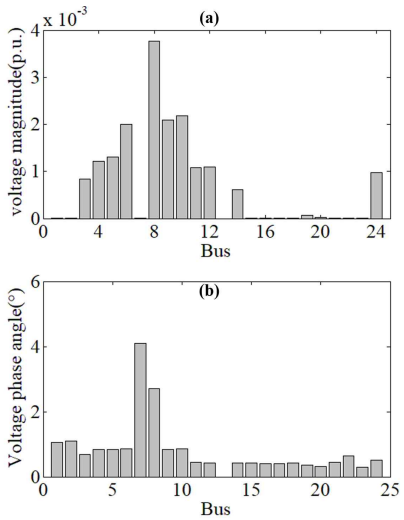

Fig. 5. Maximum differences of the expectations of bus voltage magnitude and phase angle between scenario A and scenario C

the unit's ramping limit, when the variations of wind power and loads cause an obvious climbing process in the system net load.

The maximum differences of the expectations of bus voltage magnitude and phase angle for the entire dispatching period in both scenarios are shown in Fig. 5.

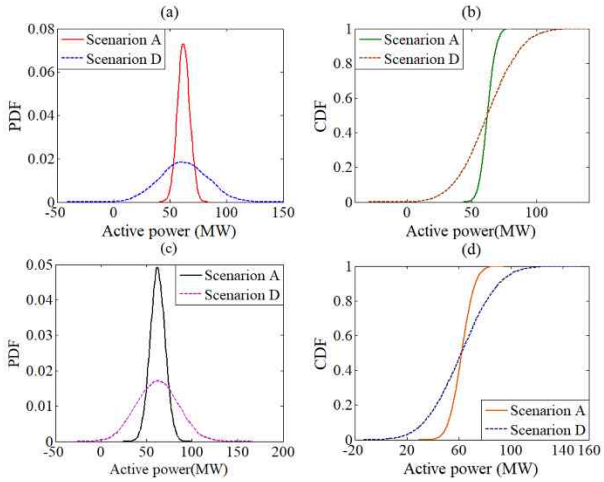

Fig. 6. PDF and CDF curves of the active power output of the slack bus

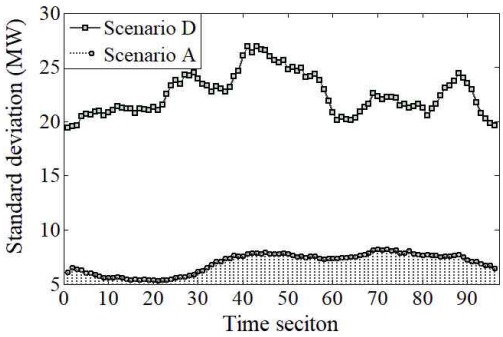

Fig. 7. Standard deviation of the active power output of the slack bus

As shown in the figure, the coupling of time sections has a significant influence on the distribution of the system state variables. The maximum difference of voltage magnitude exception is 0.0038 p.u., while the maximum difference of voltage phase angle is 4.0872°. In comparison, the bus voltage phase angles are more likely to be impacted by the dispatching strategy. This is because, different time sections are mainly coupled with each other by the active power outputs of units with a limited ramping ability, and for transmission systems, the active power has a strong relationship with the bus voltage phase angle.

4.1.3 Influence of the AGC Strategy

The PDF and CDF curves of the active power outputs of the slack buses in the minimum load time section and in the maximum load time section in Scenario A and Scenario D are shown in Fig. 6. The standard deviations of the active power outputs of the slack bus in Scenario A and Scenario D are shown in Fig. 7.

It can be observed that the standard deviation of the active power output of the slack bus in Scenario D is obviously greater than that in Scenario A. It can be observed that, due to the lack of consideration of the AGC strategy in Scenario D, the unbalanced power will be fully compensated by the slack bus alone when the wind power or loads deviate from the forecast values, which will result in a great deviation in the active power output of the slack bus. In Scenario A, because the AGC units share the imbalanced power, the deviation will be reduced. The results indicate that it is essential to consider the AGC regulation strategy in PLF.

4.2 The modified IEEE 118-bus system

The modified IEEE 118-bus system is also used to illustrate the effectiveness of the proposed method, which

Table 2. Calculation errors of the proposed method for IEEE 118-bus system

	State variables	Characteristic variables	Average value	Maximum value
Absolute error	bus voltage magnitude (p.u.)	expectation	0.0000107	0.0000673
		standard deviation	0.00000354	0.0000491
	bus voltage phase angle (°)	expectation	0.0065	0.0165
		standard deviation	0.0017	0.0094
	branch active power (MW)	expectation	0.0878	0.7365
		standard deviation	0.0197	0.1842
	branch reactive power (MVar)	expectation	0.1023	0.9902
		standard deviation	0.0743	0.8271
Relative error	bus voltage magnitude (%)	expectation	0.001061	0.0092
		standard deviation	0.5147	3.74
	bus voltage phase angle (%)	expectation	0.0723	2.945
		standard deviation	0.691	3.214
	branch active power (%)	expectation	0.0931	4.25
		standard deviation	0.7912	3.482
	branch reactive power (%)	expectation	0.2789	4.52
		standard deviation	0.2515	3.913

includes 54 thermal units and 186 branches. Based on an original system, a wind farm with a capacity of 500 MW is integrated to bus 95. Details of related parameters of the lines, loads, and generators can be found online from http://motor.ece.iit.edu/data/SCUC_118_WIND.xls. The standard deviations of the wind power forecast error and the load forecast error are 10% and 3% respectively.

For sake of limited space, the following two scenarios are considered.

Scenario E: Uses the method proposed in this paper and considers both AGC and the coupling of system states between different time sections;

Scenario F: Uses the conventional MCS method and considers both AGC and the coupling of system states between different time sections.

The sample size N in Scenario F is set to 5000. The calculation errors of the proposed method for IEEE 118-bus system are shown in Table 2. It can be observed from the table that the proposed method is of relatively high computational accuracy. Under the same computing conditions, the computing time of Scenario E is 282.3s, while that of Scenario F is 17513.6s. Therefore, the computational efficiency of the proposed method is much higher than the MCS method.

Acknowledgements

The authors greatly acknowledge the support from National Natural Science Foundation of China (NSFC) (51507108, 51337005).

5. Conclusion

The large-scale integration of wind power has made the power system face more uncertainties, causing its operation to become more and more complicated. PLF is an important tool for the probabilistic steady-state security analysis of a power system. In this paper, we proposed a PLF calculation method in which the multi-time scale dispatching features of the power systems integrated with wind power were taken into account. In this method, for the whole study period, the ramp limitation of units and the steady-state security constraints of the network were comprehensively considered. At each time section, the features of the AGC strategy were considered, and the imbalance power caused by the forecast errors of wind power and loads, were reasonably assigned. The calculation efficiency of the algorithm was ensured by the calculation method based on cumulants and the Gram–Charlier expansion. The proposed method was validated by the test results from an experiment using the IEEE RTS 24-bus system and IEEE 118-bus system. Results indicated that the coupling of different time sections had a significant effect on the probability distribution of power flow and that the deviation of the slack bus's active power caused by variations of wind power and loads could be reduced by AGC regulation.

Nomenclature

Ω_{AG} Set of conventional units involved in the AGC regulation.
Ω_{NG} Set of conventional units not involved in the AGC regulation.
Ω_{G} Set of all conventional units, $=\Omega_{\mathrm{AG}} \cup \Omega_{\mathrm{NG}}$.
Ω_{B} Set of all buses.
Ω_{W} Set of all wind farms.
Ω_{D} Set of all loads.
Ω_{L} Set of all branches.
$P_i^{\mathrm{wf}}(t)$ Forecast value of active power output of the ith wind farm at time section t.
$P_i^{\mathrm{wr}}(t)$ Actual active power output of the ith wind farm at time section t.
$\Delta e_i^{\mathrm{w}}(t)$ Forecast error of active power output of the ith wind farm at time section t.
$\sigma_i^{\mathrm{w}}(t)$ Variance of the forecast error of active power output of the ith wind farm at time section t.
Δt Interval between two adjacent time sections.
$P_i^{\mathrm{df}}(t)$ Forecast value of the ith load at time section t.
$P_i^{\mathrm{dr}}(t)$ Actual value of the ith load at time section t.
$\Delta e_i^{\mathrm{d}}(t)$ Forecast error of the ith load at time section t.
$P_i^{\mathrm{G}}(t)$ Scheduled value of active power output of the ith unit at time section t.
$\Delta P_i^{\mathrm{AG}}(t)$ Variation of the active power output of the ith AGC unit at time section t.
α_i^{AG} Participation factor of the ith AGC unit.
a_i, b_i, c_i Coefficients of power generation cost function of the ith unit.
T Number of time sections.
P_i^{Gmax} Maximum active output power of the ith unit.
P_i^{Gmin} Minimum active output power of the ith unit.
$\Delta r_i^{\max}$ Maximum ramp rate of the ith unit.
$\Delta R(t)$ Minimum spinning reserve capacity required at time section t.
$P_i^{\mathrm{L}\max}$ Maximum power flow limit of the ith branch.
$P_i^{\mathrm{L}}(t)$ Power flow of the ith branch at time section t.
$P_i(t)$ Active power injection of the ith bus at time section t.
$\Delta P_i(t)$ Variation in the injection power of the ith bus at time section t.
$\Delta \boldsymbol{P}$ Vector of injection power variations of buses except the slack bus.
$\Delta P^{\mathrm{s}}(t)$ Total system imbalance power caused by wind power and load at time section t.
$\boldsymbol{M}_{\mathrm{G2B}}$ Connectivity matrix between AGC units and buses in Ω_{B}. If the jth AGC unit is connected with the ith bus, the element at the ith row jth column of the matrix will be 1, otherwise, it will be 0.
$\boldsymbol{M}_{\mathrm{W2B}}$ Connectivity matrix between wind farms and

buses in Ω_B. If the *j*th wind farm is connected with the *i*th bus, the element at the *i*th row *j*th column of the matrix will be 1, otherwise, it will be 0.

$\boldsymbol{M}_{D2B}$ Connectivity matrix between loads and buses in Ω_B. If the *j*th load is connected with the *i*th bus, the element at the *i*th row *j*th column of the matrix will be 1, otherwise, it will be 0

n_B Number of buses in the system.

n_{PV} Number of PV buses in the system.

n_{PQ} Number of PQ buses in the system.

n_L Number of branches in the system.

n_{AG} Number of units involved in the AGC regulation.

n_W Number of wind farms.

n_D Number of loads.

$$\boldsymbol{\alpha}_{W2G} = \begin{bmatrix} \alpha_1^{AG} & \alpha_1^{AG} & \cdots & \alpha_1^{AG} \\ \alpha_2^{AG} & \alpha_2^{AG} & \cdots & \alpha_2^{AG} \\ \vdots & \vdots & \cdots & \vdots \\ \alpha_{n_{AG}}^{AG} & \alpha_{n_{AG}}^{AG} & \cdots & \alpha_{n_{AG}}^{AG} \end{bmatrix} \in \mathbf{R}^{n_{AG} \times n_W}.$$

$$\boldsymbol{\alpha}_{D2G} = \begin{bmatrix} \alpha_1^{AG} & \alpha_1^{AG} & \cdots & \alpha_1^{AG} \\ \alpha_2^{AG} & \alpha_2^{AG} & \cdots & \alpha_2^{AG} \\ \vdots & \vdots & \cdots & \vdots \\ \alpha_{n_{AG}}^{AG} & \alpha_{n_{AG}}^{AG} & \cdots & \alpha_{n_{AG}}^{AG} \end{bmatrix} \in \mathbf{R}^{n_{AG} \times n_D}.$$

$\boldsymbol{S}$ Vector of active power and reactive power injections of buses except the slack bus, $\boldsymbol{S} \in \mathbf{R}^{2(n_B-1)}$.

$\boldsymbol{X}$ Vector of bus state variables, including the bus voltage magnitude and phase angle of PQ buses and the phase angle of PV buses, $\boldsymbol{X} \in \mathbf{R}^{n_{PV}+2n_{PQ}}$.

$\boldsymbol{Z}$ Vector of system branch power flow, $\boldsymbol{Z} \in \mathbf{R}^{2n_L}$.

$\Delta\boldsymbol{S}$ Vector of variations in the bus injection power.

$\Delta\boldsymbol{X}$ Vector of variations in bus voltage magnitude and phase angle.

$\Delta\boldsymbol{Z}$ Vector of variations in system branch power flow.

$\boldsymbol{f}$ Equations of the bus power injection functions.

$\boldsymbol{g}$ Equations of the branch power flow functions.

References

[1] A. M. Foley, P. G. Leahy, A. Marvuglia, and E. J. Mckeogh, "Current methods and advances in forecasting of wind power generation," *Rene. Energy*, vol. 27, no. 1, 2012.

[2] Y. V. Makarov, C. Loutan, J. Ma, and P. de Mello, "Operational impacts of wind generation on California power systems," *IEEE Trans. Power Syst*., vol. 24, no. 2, pp. 1039-1050, May 2009.

[3] A. M. Leita da Silva, S. M. P. Ribeiro, V. L. Arienti, R. N. Allan, and M. B. Do Coutto Filho, "Probabilistic load flow techniques applied to power system expansion planning," *IEEE Trans. Power Syst*., vol. 5, no. 4, pp. 1047-1053, Nov. 1990.

[4] N. D. Hatziaryriou, and T. S. Karakatsanis, "Probabilistic load flow for assessment of voltage instability," *IEE Proc. Gener., Transm., Distrib*., vol. 145, no. 2, pp. 196-202, 1998.

[5] Y. Y. Hong, and Y. F. Luo, "Optimal VAR control considering wind farms using probabilistic load-flow and Gray-based Genetic Algorithms," *IEEE Trans. Power Del*., vol. 24, no. 3, pp. 1441-1449, Jun. 2009.

[6] J. M. Sexauer, and S. Mohagheghi, "Voltage quality assessment in a distribution system with distributed generation - a probabilistic load flow approach," *IEEE Trans. Power Del*., vol. 28, no. 3, pp. 1652-1662, Jul. 2013.

[7] B. Borkowska, "Probabilistic load flow," *IEEE Trans. Power App. Syst*., vol. PAS-93, no. 3, pp. 752-759, 1974.

[8] H. Yu, C. Y. Chung, K. P. Wong, H. W. Lee, and J. H. Zhang, "Probabilistic load flow evaluation with hybrid Latin hypercube sampling and Cholesky decomposition," *IEEE Trans. Power Syst*., vol. 24, no. 2, pp. 661-667, May, 2009.

[9] J. M. Morales, L. Baringo, A. J. Conejo, and R. Minguez, "Probabilistic power flow with correlated wind sources," *IET Gener. Trasmiss. Distrib*., vol. 4, no. 5, pp. 641-651, May 2010.

[10] C. L. Su, "Probabilistic load-flow computation using point estimate method," *IEEE Trans. Power Syst*., vol. 20, no. 4, pp. 1843-1851, Nov, 2005.

[11] J. M. Morales, and J. P. Ruiz, "Point estimate schemes to solve the probabilistic power flow," *IEEE Trans. Power Syst*., vol. 22, no. 4, pp. 1594-1601, Nov, 2007.

[12] P. Caramia, G. Carpinelli, and P. Varilone, "Point estimate schemes for probabilistic three-phase load flow," *Elect Power Syst. Res*., vol. 80, no. 2, pp. 168-175, 2010.

[13] C. Wan, Z. Xu, Z. Y. Dong, and K. P. Wong, "Probabilistic load flow computation using First-order Second-moment method," *IEEE PESGM*, July 2012, pp. 1-8.

[14] R. N. Allan, and M. R. G. Al Shakarchi, "Probabilistic AC load flow," *Proc. IEE*, vol. 123, no. 6, pp. 531-536, Jun. 1976.

[15] R. N. Allan, C. H. Grigg, and M. R. G. Al-Shakarchi, "Numerical techniques in probabilistic load flow problems," *Int. J. Numer. Meth. Eng*., vol. 10, pp. 853-860, Mar. 1976.

[16] P. Zhang and S. T. Lee, "Probabilistic load flow computation using the method of combined cumulants and Gram-Charlier expansion," *IEEE Trans. Power Syst*., vol. 19, no. 1, pp. 676-682, Feb. 2004.

[17] T. Williams, and C. Crawford, "Probabilistic load flow modeling comparing maximum Entropy and Gram-Charlier probability density function reconstructions," *IEEE Trans. Power Syst*., vol. 28, no. 1, pp. 272-280, Feb. 2013.

[18] J. Usaola, "Probabilistic load flow in systems with wind generation," *IET Gen., Transm., Distrib*., vol. 3, no. 12, pp. 1031-1041.
[19] N. D. Hatziargyriou, T. S. Karakatsanis, and M. Papadopoulos, "Probabilistic load flow in distribution systems containing dispersed wind power generation," *IEEE Trans. Power Syst*., vol. 8, no. 1, pp. 159-165, Feb. 1993.
[20] D. Villanueva, J. L. Pazos, and A. Feijoo, "Probabilistic load flow including wind power generation," *IEEE Trans. Power Syst*., vol. 26, no. 3, pp. 1659-1667, 2011.
[21] Y. Yuan, J. Zhou, P. Ju, and J. Feuchtwang, "Probabilistic load flow computation of a power system containing wind farms using the method of combined cumulants and Gram-Charlier expansion," *IET Renew. Power Gener*., vol. 5, no. 6, pp. 448-454, 2011.
[22] M. H. Ahmed, K. Bhattacharya, and M. M. A. Salama, "Probabilistic distribution load flow with different wind turbine models," *IEEE Trans. Power Syst*., vol. 28, no. 2, pp. 1540-1549, May 2013.
[23] Z. Ren, W. Li, R. Billinton, and W. Yan, "Probabilistic power flow analysis based on the stochastic response surface method," *IEEE Trans. Power Syst*., vol. 31, no. 3, pp. 2307-2315, May 2016.
[24] M. Fan, V. Vittal, G. T. Heydt, R. Ayyanar, "Probabilistic power flow analysis with generation dispatch including photovoltaic resources," *IEEE Trans. Power Syst*., vol. 28, no. 2, pp. 1797-1805, May 2013.
[25] Reliability Test System Task Force of the Application of Probability Methods Subcommittee, "IEEE reliability test system," *IEEE Trans. Power App. Syst*., vol. PAS-98, no.6, pp. 2047-2054, 1979.
[26] C. Wang, and S. M. Shahidehpour, "Effects of ramp-rate limits on unit commitment and economic dispatch," *IEEE Trans. Power Syst*., vol. 8, no. 3, pp. 1341-1350, Aug. 1993.

Chao Qin He received his B.S., M.S. and Ph.D. degrees in Electrical Engineering from Tianjin University in 2009, 2011 and 2014 respectively. After that he has been a lecturer of School of Electrical Engineering and Automation at Tianjin University. His research interests include economic dispatch and power system security and stability analysis.

Yixin Yu He received his B.S. and M.S. degrees in electrical engineering from Tianjin University, China, in 1958 and 1963, respectively. He became a full professor at Tianjin University in 1985. He was a visiting scholar in the Department of EECS, University of California, Berkeley, from 1980 to 1982, and a Chair Visiting Professor of Kyushu Institute of Technology, Japan, from 1995 to 1997. His research areas include power system stability and security, power distribution planning, and the Smart Grid. In 2005, Prof. Yu was elected as an Academician of the Chinese Academy of Engineering.

Yuan Zeng He received his B.S. and Ph.D. degrees all in electrical engineering form Tianjin University in 1997 and 2003, respectively. He is now an associate professor of Tianjin University. His interests include power system stability and security analysis, power grid planning, risk assessment and smart grid.